

1
2
3
4
5
6
7
8
9
10
11
12
13
14
15
16
17
18
19
20
21
22
23
24
25
26
27
28
29
30
31
32
33
34
35
36
37
38
39
40
41
42
43
44
45
46

The OPFOS microscopy family: High-resolution optical-sectioning of biomedical specimens

Jan A.N. Buytaert^{1,°}, Emilie Descamps², Dominique Adriaens²,
and Joris J.J. Dirckx¹

¹ Laboratory of BioMedical Physics – University of Antwerp,
Groenenborgerlaan 171, B-2020 Antwerp, Belgium

² Evolutionary Morphology of Vertebrates – Ghent University,
K.L. Ledeganckstraat 35, B-9000 Gent, Belgium

[°] Corresponding author:
email jan.buytaert@ua.ac.be;
telephone 0032 3 265 3553;
fax 0032 3 265 3318.

Abstract

47
48
49
50
51
52
53
54
55
56
57
58
59
60
61
62
63
64
65
66
67
68
69
70
71
72
73
74
75
76
77
78
79
80
81
82
83
84
85
86
87
88
89
90
91
92
93

We report on the recently emerging (Laser) Light Sheet based Fluorescence Microscopy field (LSFM). The techniques used in this field allow to study and visualize biomedical objects non-destructively in high-resolution through virtual optical sectioning with sheets of laser light. Fluorescence originating in the cross section of the sheet and sample is recorded orthogonally with a camera.

In this paper, the first implementation of LSFM to image biomedical tissue in three dimensions – Orthogonal-Plane Fluorescence Optical Sectioning microscopy (OPFOS) – is discussed. Since then many similar and derived methods have surfaced (SPIM, Ultramicroscopy, HR-OPFOS, mSPIM, DSLM, TSLIM, ...) which we all briefly discuss. All these optical sectioning methods create images showing histological detail.

We illustrate the applicability of LSFM on several specimen types with application in biomedical and life sciences.

Keywords

serial sectioning, OPFOS, LSFM, optical sectioning, fluorescence, three-dimensional imaging, biomedical

94 **Introduction**

95
96 Serial (Mechanical) Histological Sectioning (SHS) creates physical slices of fixed, stained and
97 embedded tissues which are then imaged with an optical microscope in unsurpassed sub-
98 micrometer resolution. Obtaining these slices is however extremely work-intensive, requires
99 physical (one-time and one-directional) slicing and thus destruction of the specimen. A 2-D
100 sectional image reveals lots of histologically relevant information, but a data stack and its 3-
101 D reconstruction are even more essential for the morphological interpretation of complex
102 structures, because they give additional insight in the anatomy. The SHS method requires
103 semi-automatic to manual image registration to align all recorded 2-D slices in order to get
104 realistic 3-D reconstructions. Often dedicated image processing of the sections is needed
105 because of the geometrical distortions from the slicing.

106
107 A valuable alternative to achieve sectional imaging and three-dimensional modeling of
108 anatomic structures can be found in the little known and relatively recent field of
109 microscopy called (Laser) Light Sheet based Fluorescence Microscopy or LSFM. These non-
110 destructive methods generate registered optical sections in real-time through bio(medical)
111 samples ranging from microscopic till macroscopic size. LSFM can reveal both bone and soft
112 tissue at a micrometer resolution, thus showing a large amount of histological detail as well.

113
114 The first account of the LSFM idea was published by Voie, Burns and Spelman in 1993 and
115 applied to image the inner ear cochlea of guinea pig [1]. Their method was called
116 Orthogonal-Plane Fluorescence Optical Sectioning (OPFOS) microscopy or tomography. The
117 motivations for the OPFOS invention were (1) the above mentioned disadvantages of serial
118 histological sectioning, (2) the typical photo-bleaching of fluorophores in conventional or
119 confocal fluorescence microscopy, and (3) the fact that samples are optically opaque which
120 means a limited penetration depth and inefficient delivering and collecting of light.

121
122 Surprisingly, all these problems can be avoided by combining two old techniques. Voie and
123 colleagues first combined the Spalteholz method of 1911 [2] with the even older
124 Ultramicroscope method of 1903 [3]. In most microscopy techniques, the same optical path
125 and components are used for the illumination and the observation of light. Siedentopf and
126 Nobel Prize winner Zsigmondy made a simple change of the optical arrangement in their
127 Ultramicroscopy setup by separating the illumination and viewing axis [3]. Furthermore,
128 their illumination was performed by a thin plane or sheet of light. Orthogonal viewing or
129 observation of this sheet offers full-field and real-time sectional information. Their method
130 was originally developed for gold particle analysis in colloidal solutions with sunlight. OPFOS
131 used the same optical arrangement but for tissue microscopy. The separation of the
132 illumination and imaging axis combined with laser light sheet illumination only illuminates
133 the plane that is under observation (in contrast to confocal microscopy) and thus avoids
134 bleaching in sample regions that are not being imaged. Generally, samples are optically
135 opaque so the plane of laser light cannot section the sample. Spalteholz introduced a
136 clearing method which dates back exactly 100 years [2]. His museum technique is capable of
137 making tissue transparent by matching the refractive index throughout the entire object
138 volume by means of a mixture of oils with refractive indices close to that of protein.
139 Submerged in this Spalteholz fluid, a prepared specimen appears invisible, with light passing
140 right through it unscattered and without absorption. This clearing or refractive index

141 matching is essential for the OPFOS technique to achieve a penetration depth of several
142 millimeters. This procedure is followed by staining of the sample with fluorescent dye or just
143 by just relying on naturally occurring auto-fluorescence. The sectioning laser plane activates
144 the fluorophores in the cross section of sheet and sample, which are finally orthogonally
145 recorded by a camera.

146
147 OPFOS utilizes yet a third method in conjunction with the two previous techniques when the
148 specimen contains calcified tissue or bone. In this case, the calcium first needs to be
149 removed before the Spalteholz procedure is applied. Bone cannot be made transparent, as
150 the calcium atoms strongly scatter light.

151
152 Since 1993, many OPFOS-like derived methods were developed for tissue microscopy, all
153 based on light sheet illumination. 'LSFM' has become a broadly accepted acronym to cover
154 the whole of these techniques, coined in Dresden (Germany) 2009. In the discussion, we will
155 give a short overview of this OPFOS-derived LSFM microscopy family. First, we will explain in
156 detail the specimen preparation and the optical arrangement of the original OPFOS setup.
157 The remainder of this paper will serve to demonstrate some applications of OPFOS.

158
159

160 **Materials and Methods**

161

162 **Specimen preparation**

163 In most LSFM methods, the biomedical tissue samples are severely limited in size, though for
164 instance the LSFM implementations of Ultramicroscopy, HR-OPFOS and TSLIM (cf. the
165 discussion section) are capable of imaging macroscopic samples up to tens of millimeters [4].
166 In all cases, an elaborate specimen preparation is required:

- 167 • Euthanasia: Living animals cannot be used in combination with clearing solutions. In
168 general, LSFM is thus mainly used *in vitro*. Clearing can be omitted and living animals
169 can be used if the species possesses a natural transparency at a certain
170 developmental stage, for instance fish embryos [5,6]. The embryos are immobilized
171 by embedding in agarose.
- 172 • Perfusion: Before dissecting a sample to the required dimensions, transcordial
173 perfusion with phosphate buffered saline is useful as coagulated blood is difficult to
174 clear with Spalteholz fluid [7-9]. If perfusion is omitted, bleaching is required.
- 175 • Fixation: Immersion in 4% paraformaldehyde (10% formalin) during 24h for
176 preservation and fixation of the specimen.
- 177 • Bleaching: Optional bleaching in 5% to 10% hydrogen peroxide for one or more days
178 can be performed when the sample contains dark pigmented tissue (e.g. black skin,
179 fish eyes) [10]. This step can also be applied after decalcification [11].
- 180 • Decalcification: When the specimen contains calcified or mineralized tissue, such as
181 cartilage or bone, decalcification is in order. A 10% demineralized water solution of
182 dihydrate ethylenediaminetetraacetic acid (EDTA) slowly diffuses calcium atoms from
183 the sample through a chelation process. Low power microwave exposure (without
184 heating) drastically accelerates the decalcification process from a month to several
185 days [12,13].

- 186
- 187
- 188
- 189
- 190
- 191
- 192
- 193
- 194
- 195
- 196
- 197
- 198
- 199
- 200
- 201
- 202
- 203
- 204
- 205
- 206
- 207
- 208
- 209
- Dehydration: Immersion in a graded ethanol series (f.i. 25%, 50%, 75%, 100%, 100% each for 24h) removes all water content from the sample [12]. In the final 100% step, optional addition of anhydrous copper sulfate at the bottom of the ethanol bath might improve the dehydration [14].
 - Hexane or benzene: The optional immersion in a graded series of hexane or benzene is said to improve dehydration further [8,11,14,15]. Furthermore, hexane might assist in clearing myelin present in the tissue sample. Nerve axons are surrounded by myelin sheets which do not easily become transparent with Spalteholz fluid.
 - Clearing: To achieve large volume imaging in inherently less transparent samples, clearing is needed. The specimen are to be immersed in clearing solution, either through a graded series (f.i. 25%, 50%, 75%, 100%, 100% each for 24h) when the hexane or benzene step was skipped [12], or directly in 100% pure clearing solution when hexane or benzene were applied [8,11]. The clearing solution mimics the refraction index of protein and matches the refraction index of the sample to the solution. The solution can either consist of pure benzyl benzoate followed in a later stage by the final mixture [14], or directly of this mixture solution. A 5:3 mixture of methyl salicylate and benzyl benzoate is called Spalteholz fluid [1,2,7]. For brain tissue, a 1:2 mixture of benzyl alcohol and benzyl benzoate has been found to give better results [8,11].
 - Staining: The required fluorescence can originate from auto-fluorescence from lipofuscins, elastin and/or collagen [8]. Fluorescent staining can be applied by immersion in a dye bath (of f.i. Rhodamine B isothiocyanate in clearing solution [1]) or even by functional staining. However, many fluorescent dyes deteriorate or even break down completely because of the aggressive clearing solution used, e.g. GFP.

210
211

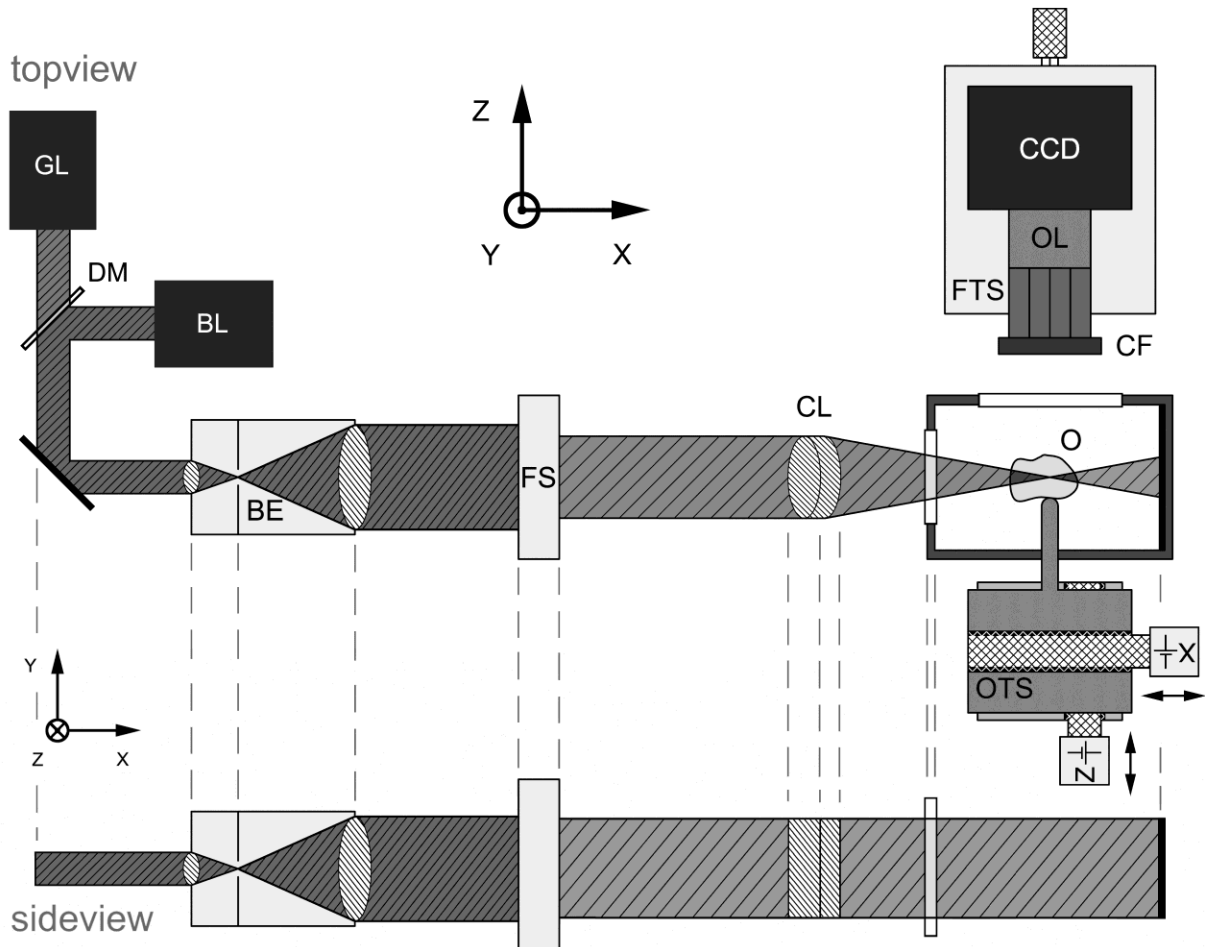
212 **Optical setup**

213 In what follows, the original OPFOS setup is discussed as it was introduced by Voie et al. in
214 1993 [1]. Many improved versions have been developed since, all based on the OPFOS or
215 Ultramicroscopy design (cf. the discussion).

216

217 The setup is represented in Figure 1 and Figure 2. The prepared sample is illuminated by an
218 XY-sheet of laser light travelling along the X-axis. The omni-directional fluorescence light
219 emitted in the positive Z-axis is used for imaging. Virtual section images in the XY-plane are
220 hence recorded; by translation of the specimen along the Z-axis, an aligned sequence of
221 section images is obtained.

222
223



224
225
226
227
228
229
230
231
232
233
234

Figure 1. Schematic drawing of the (HR-)OPFOS setup: Light from a green (GL) or blue laser (BL) passes through a Keplerian beam expander (BE) with spatial filter, a field stop (FS) and a cylindrical achromat lens (CL) which focuses the laser along one dimension within the transparent and fluorescent object (O). A two-axis motorized object translation stage (OTS) allows scanning of the specimen and imaging of different depths. The fluorescence light emitted by the object, is projected onto a CCD-camera by a microscope objective lens (OL) with fluorescence color filter (CF) in front. The focusing translation stage (FTS) is used to make the objective lens focal plane coincide with the laser focus.



235
236
237
238
239

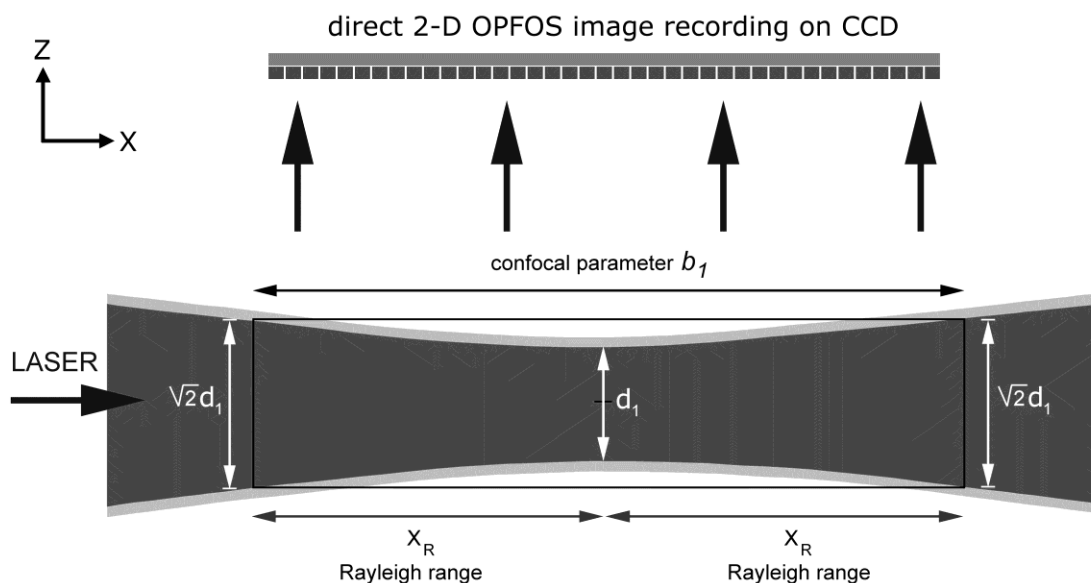
Figure 2. A 3-D setup representation of an (HR-)OPFOS setup with two-sided cylindrical lens sheet illumination, and with two laser wavelengths (green and blue). The blue laser is active here.

240 An essential requirement for OPFOS is the generation of a laser light sheet. In practice, it is
 241 impossible to generate a perfect plane or sheet of light; however, using a cylindrical lens a
 242 sheet can be approximated. A Gaussian laser beam is first expanded and collimated by a
 243 Keplerian beam expander. The broadened beam then travels along the X-axis through a
 244 cylindrical lens which focuses light in only one dimension to a line along the Z-axis. Along the
 245 Y-axis the Gaussian beam is unaltered, cf. Figure 1. In the XZ-plane, the light sheet has a
 246 hyperbolic profile in the focal zone, cf. Figure 3. The Z-thickness of the profile increases in
 247 either way along the X-axis when moving away from the minimal beam waist focus d_1 . The
 248 Rayleigh range x_R is the distance on either site of the minimal focus d_1 where the
 249 hyperbolically focused beam has thickened to $\sqrt{2} d_1$. This variable is described by the

250 expression $b_1 = 2x_R = \frac{\pi d_1^2}{2\lambda}$, where b_1 is called the confocal parameter or the total distance
 251 in which a focus smaller than $\sqrt{2}d_1$ is maintained. The numerical aperture of the cylindrical
 252 lens is inversely related to the confocal parameter b_1 and directly proportional to the beam
 253 waist focal thickness d_1 .

254
 255 The height of the beam in Y-direction combined with the confocal parameter b_1 along the X-
 256 axis defines the size of the XY-sheet which sections the sample. The specimen consequently
 257 has to fit within this zone. A trade-off exists between maximal image and sample width ($\approx b_1$)
 258 and the sectioning thickness $\sqrt{2} d_1$ ($\sim 1/\sqrt{b_1}$).

259
 260
 261
 262
 263



264 **Figure 3.** The hyperbolic focus profile of a cylindrical lens is shown. OPFOS records 2-D images in an
 265 approximated planar sheet defined by the confocal parameter zone b_1 where the thickness is considered
 266 constant at $\sqrt{2}d_1$. The dark gray area in the center represents the $1/e^2$ intensity profile.
 267

268
 269

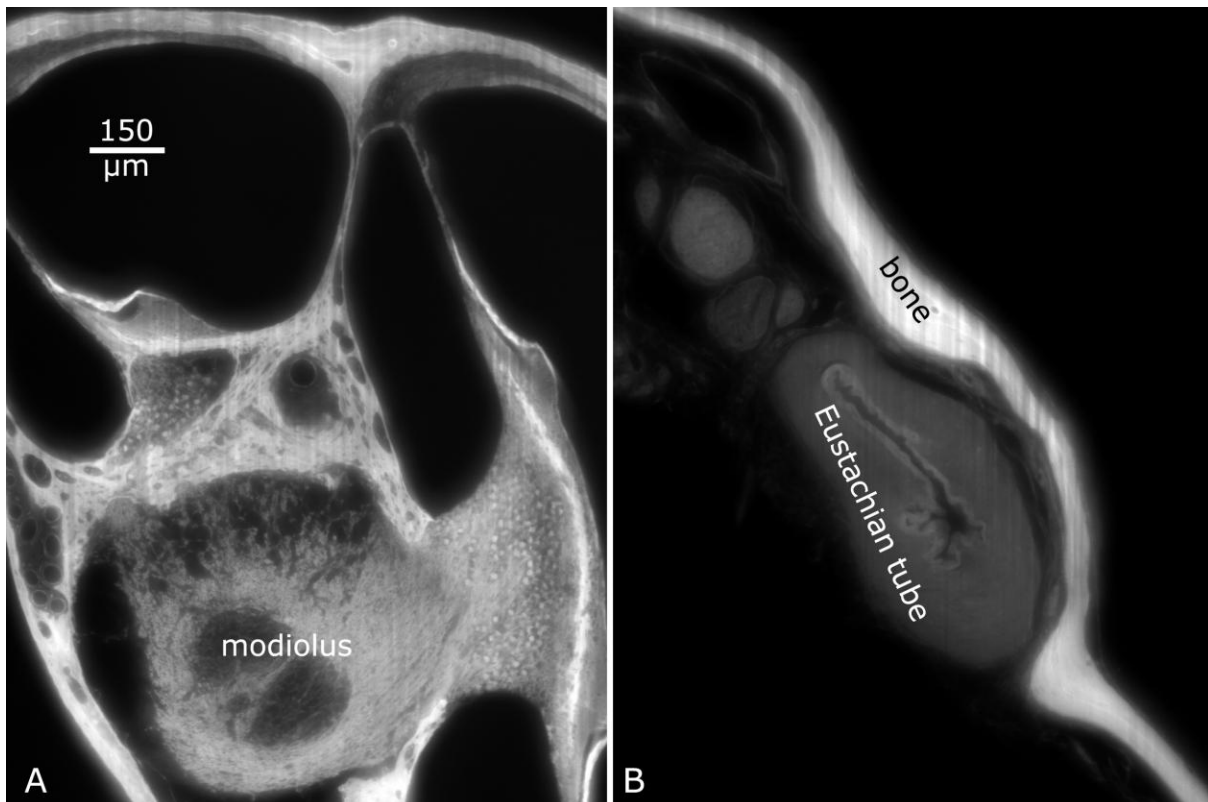
270 In summary, an OPFOS image has a slicing thickness d_1 in the center, growing to $\sqrt{2} d_1$ at the
271 edges x_R . Everything within the thickness of the laser light sheet is integrated into a flat
272 section image, so actually a varying thickness and slicing resolution is integrated in the 2-D
273 image. The wavelength of the laser light depends on the fluorophore that is to be excited. A
274 green laser (532 nm) is suited to excite Rhodamine B, while the blue laser (488 nm) is suited
275 to evoke autofluorescence in many biomedical tissue samples.
276
277

278 Results and Discussion

279 Application examples

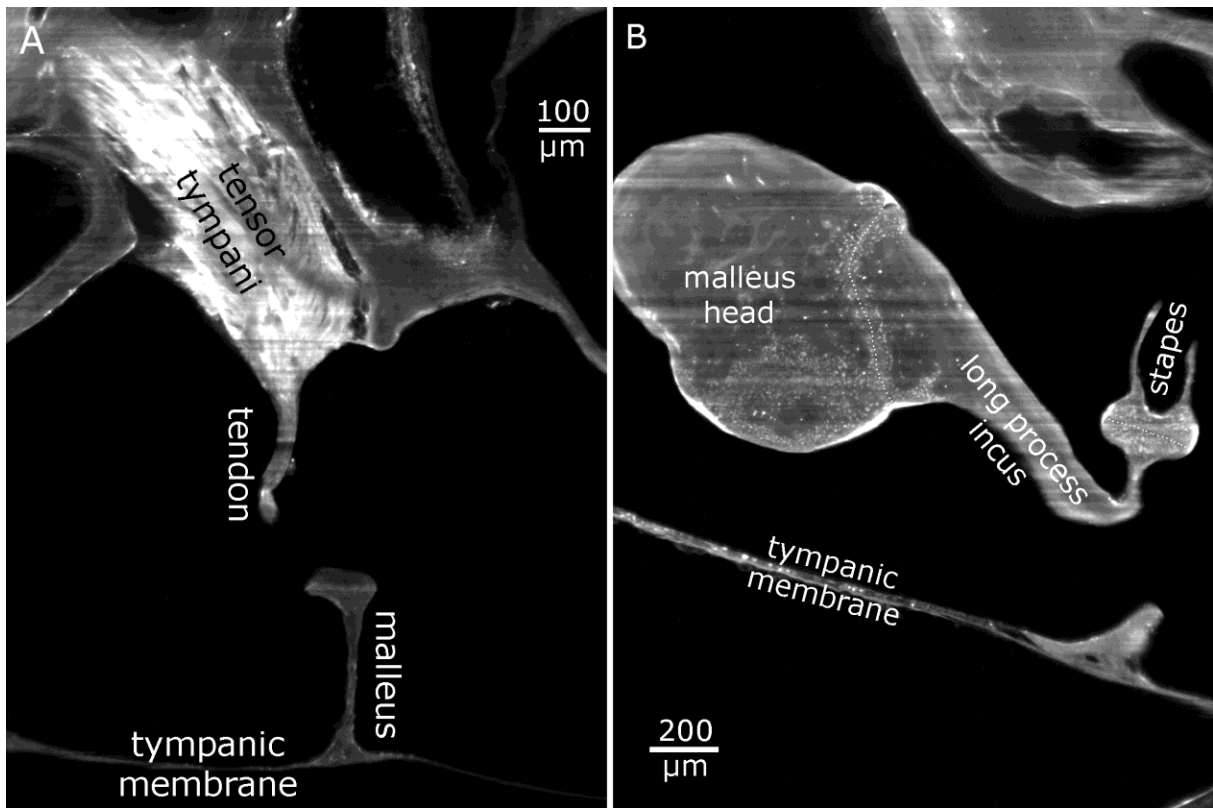
280 Biomechanics of hearing

281 As a first illustration of the above described OPFOS setup, we show an application in hearing
282 research of the middle ear [16]. Better understanding of the biomechanics of hearing
283 through finite-element modeling requires accurate morphology of the hearing bones and
284 their suspensory soft tissue structures. In Figure 4 and Figure 5, OPFOS cross sections in
285 gerbil (*Meriones unguiculatus*) middle ears are shown, which can be segmented and
286 triangulated into 3-D surface mesh models, cf. Figure 6. Thanks to the OPFOS technique, the
287 sections through the sample can be visualized in real-time and clearly show histological
288 detail on both bone and soft tissue.
289
290



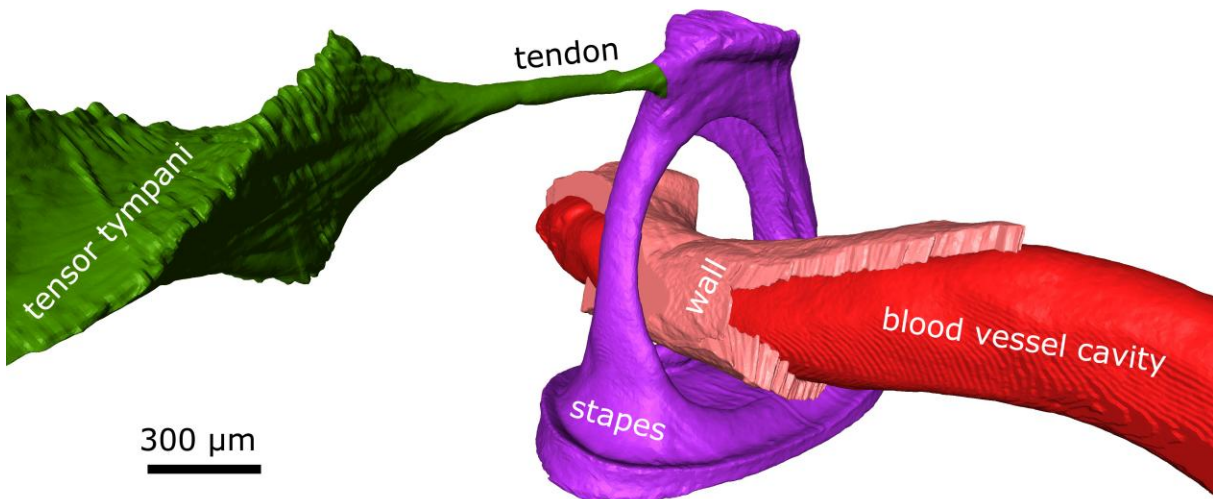
291
292 **Figure 4.** An OPFOS cross section of 1600x1200 pixels through (A) the scalae and modiolus of a gerbil inner ear
293 cochlea and (B) a closed Eustachian tube in the middle ear. Rhodamine staining was combined with 532nm
294 laser light sheet sectioning.

295
296



297
298
299
300
301
302
303
304

Figure 5. 2-D virtual cross sections (1600x1200 pixels) from OPFOS microscopy on the gerbil middle ear. **(A)** Tensor tympani muscle and tendon reaching down towards the malleus hearing bone. **(B)** Incudomalleolar and incudostapedial articulation between incus and malleus hearing bone. Rhodamine staining was combined with 532nm laser light sheet sectioning. Pixel size 1.5x1.5 μm.



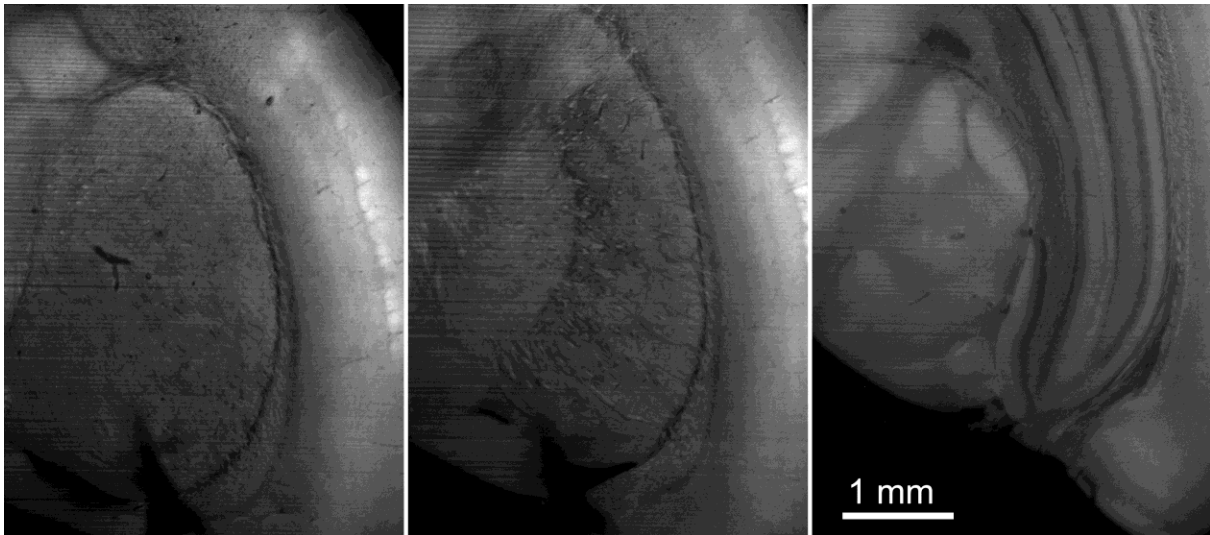
305
306
307
308
309
310
311

Figure 6. A 3-D OPFOS reconstruction showing a surface mesh of the stapes hearing bone, a blood vessel running through it, and the tensor tympani muscle attaching to the stapes head. The blood vessel wall and inner cavity are both separately modeled. Voxel size 1.5x1.5x5 μm.

312 Morphology of the brain

313 In neurology, morphological brain atlases are a useful tool. To this end, sectional imaging
314 with histological detail of mice (C57 black *Mus musculus*) brain can be achieved with the
315 OPFOS method, cf. Figure 7. The brain was cleared using the Spalteholz method, though for
316 better results a combination of benzyl alcohol and benzyl benzoate could be used (cf. the
317 section on specimen preparation). An extra hexane immersion step might further improve
318 clearing of the brain.

319
320

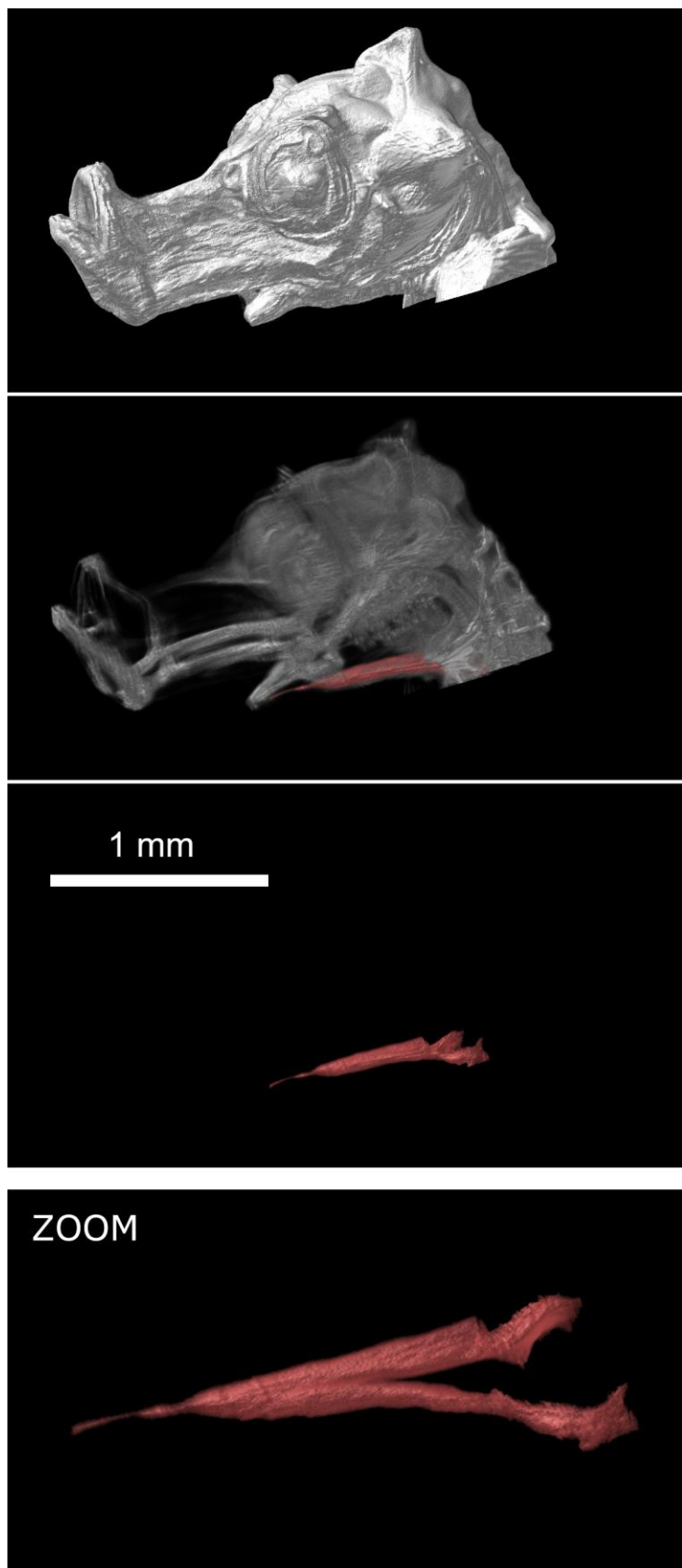


321
322 **Figure 7.** Three OPFOS cross sections of 1600x1200 pixels at different depths in a mouse brain. Natural
323 autofluorescence of the brain was achieved using 488 nm laser light sheet sectioning. Pixel size 3x3 μm .
324
325

326 Biomechanics of small vertebrates

327 In morphological studies, functionality of a musculoskeletal system requires the visualization
328 of both skeleton and muscles. For example, to gain insight in the feeding mechanisms of
329 newly born seahorses (*Hippocampus reidi*), the shape, volume and orientation of the
330 sternohyoideus muscle is, among other structures, of special interest (Figure 8). This
331 conspicuous muscle spans from the shoulder girdle to the hyoid bar, assisting in an
332 extremely rapid feeding strike in order to suck in prey [17].

333

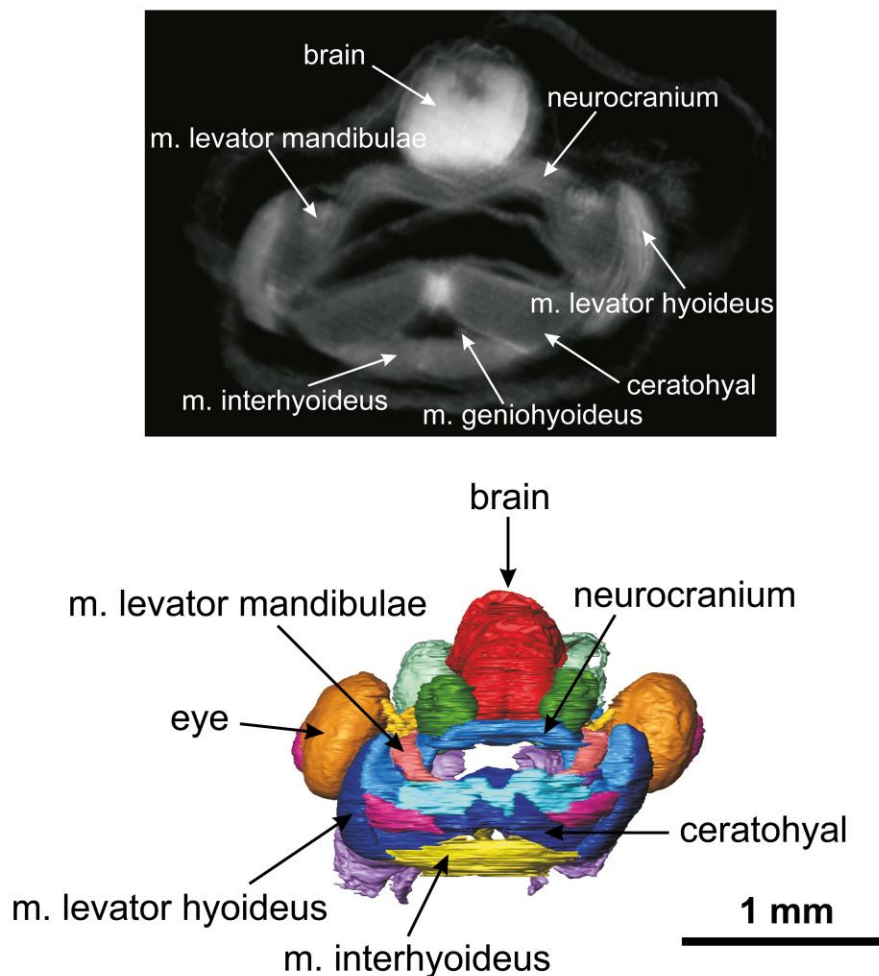


334
335
336
337
338
339

Figure 8. 3-D reconstruction of the head of a one-day old seahorse. The OPFOS image data is functionally segmented to study the morphology of the sternohyoideus muscle, cf. zoom (oblique view of the muscle). Natural autofluorescence of the head was achieved using 488 nm laser light sheet sectioning. Voxel size 3.5x3.5x5 μm .

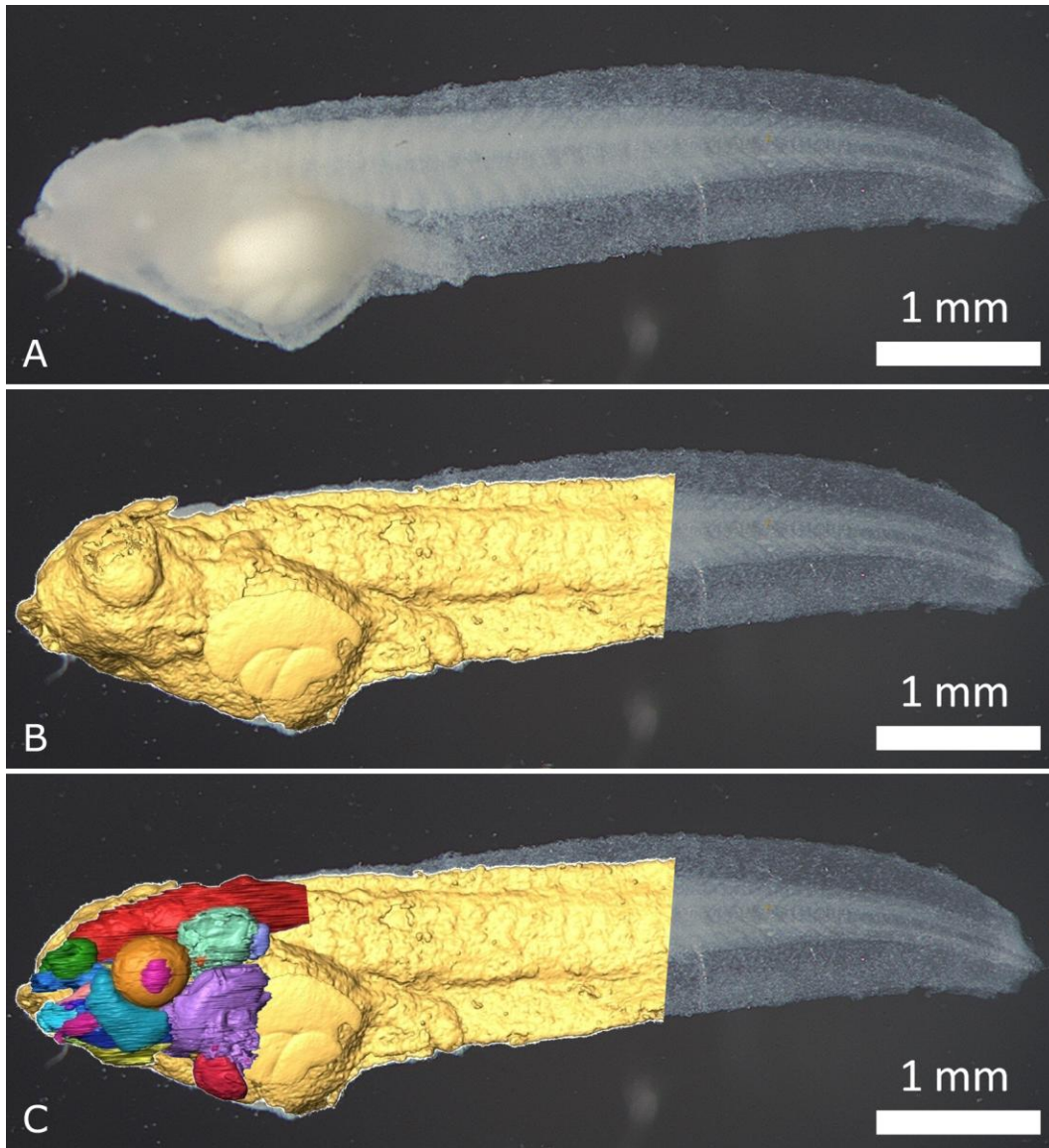
340
341
342
343
344
345
346
347
348
349
350
351

Organogenesis and evolutionary morphology can benefit from OPFOS as well. The technique allows to discern the main structural elements of the head of an African clawed tadpole (*Xenopus laevis*) without any dissection. All different tissue types, such as muscle, skeletal and nervous tissues could be visualized and discriminated by their distinct (auto)fluorescence gray scales, cf. Figure 9. Skeletal structures were depicted as the darkest mass, corresponding to the lowest autofluorescence. By contrast, the nervous system (brain) was the brightest part, and to a lesser extent also the muscles showed high fluorescence. A 3-D reconstruction based on the gray scales in the OPFOS image stacks illustrates this in Figure 9 and Figure 10.



352
353
354
355
356
357

Figure 9. (Top) A transverse OPFOS cross section through a tadpole head with indications of the different tissue types. **(Bottom)** A 3-D reconstruction of the entire functionally segmented OPFOS image data stack (sensory organs, muscles, cartilage and neuronal structures in different colors) (frontal view). Voxel size $1.5 \times 1.5 \times 3 \mu\text{m}$.



358
359
360
361
362
363

Figure 10. (A) A photograph of the tadpole after bleaching. (B) The photograph is superposed with the OPFOS surface mesh of the tadpole head and body. (C) Color coded functional segmentation of individual organs, cf. Figure 9.

364 **LSFM drawbacks**

365 The elaborate specimen preparation required in OPFOS and other LSFM techniques is a
366 major disadvantage. The method is considered non-destructive, however, dehydration
367 removed all water content and decalcification did the same with calcium. It is clear that
368 shrinkage is thus unavoidable and in the same order of magnitude as serial histological
369 sectioning [16,18,19].

370

371 The accuracy of measurements based on OPFOS sections depends greatly on the quality of
372 the transparency of the sample, and thus on the bleaching, dehydration and decalcification
373 process. Dark or dense regions in the sample, remaining water content or calcium atoms
374 refract or scatter laser light, leading to out-of-focus illumination and blurring. Furthermore,
375 the illuminating light sheet entering the sample from one side can be partially absorbed in

376 dense regions resulting in loss of excitation light and fluorescence on the far side of the
377 region. Remaining pigment or zones of less(er) transparency also create this kind of
378 shadows. These stripes or shadow line artifacts are a typical drawback of OPFOS-like
379 techniques. Solutions for these stripes have been implemented, cf. the following section.

380

381 Finally, it is important to keep the distance and the amount of refractive material constant
382 between the laser light sectioning plane and the observation lens when sectioning different
383 depths. By translating the refraction-index-matched sample within the Spalteholz-filled
384 specimen chamber orthogonally to the light sheet [5,7], or by rotating it within the chamber
385 [1,12], this condition is fulfilled. However, when the entire specimen holder is moved to scan
386 an image stack, the focus will degrade as the focal plane and sectioning plane no longer
387 match [8].

388

389 **The OPFOS family**

390 Optical sectioning with a plane of light was initiated in 1903 by Siedentopf and Zsigmondy
391 [3]. Their Ultramicroscopy light sheet idea was revived 90 years later by Voie et al. with the
392 OPFOS microscope [1,12,20]. This invention initiated the LSFM field but awareness and
393 growth of the field only followed after the 2004 publication of the Single or Selective Plane
394 Illumination Microscope (SPIM) in *Science* by Huisken et al. [5]. Before in 2002, Fuchs et al.
395 also built an LSFM device but not for tissue sectioning microscopy [21]. Their Thin Laser Light
396 Sheet Microscope (TLSM) was used for identification of aquatic microbes in oceanic
397 seawater (rather in the manner of Zsigmondy's Ultramicroscope for colloidal gold particles
398 [22]). The SPIM implementation was developed at Stelzer's EMBL lab in Heidelberg
399 (Germany) and quickly led to many new and improved designs. The SPIM authors claim to
400 have invented light sheet illumination and orthogonal observation independently from
401 Ultramicroscopy and OPFOS – though being aware of and citing OPFOS in 1995 [23] – based
402 on their work on oblique confocal (theta) microscopy [24]. SPIM omits the Spalteholz
403 clearing method which allows to use living animal embryos that possess a natural degree of
404 transparency, like Medaka (*Oryzias latipes*) and fruit fly (*Drosophila melanogaster*) embryos
405 embedded in agarose. Sometimes multiple SPIM image stacks are recorded between which
406 the sample was rotated, and post-processing combines them into one high-quality multiview
407 reconstruction.

408

409 In 2007, Dodt et al. published a new LSFM setup in *Nature Methods*, again called
410 Ultramicroscopy in honor of Zsigmondy, countering the inherent problem of stripe artifacts.
411 The authors added optical components to illuminate the sample simultaneously from
412 opposing sides, effectively reducing the presence of stripes in the images. The Dodt group
413 focuses on visualizing brain tissue. The same year Huisken et al. also started implementing
414 bi-directional sheet illumination (and two constantly pivoting cylindrical lenses) to reduce
415 these stripes, but his multidirectional SPIM or mSPIM setup measures each light sheet
416 consecutively [6]. The resulting two image datasets are computationally combined yielding
417 an image with minimal stripes. Another innovation in mSPIM is related to the quality of light
418 sheet illumination. Each mSPIM cylindrical lens focuses laser light to a horizontal line into the
419 back focal plane of microscope objective lens. Hence, the quality and aberrations of the light
420 sheet is determined by the well-corrected objective and not by the cylindrical lens.

421

422 Whenever using cylindrical lenses for light sheet generation, the resulting parabolic focus
423 can only be approximated as a plane over a length described by the confocal parameter, cf.
424 the section on OPFOS setup. The minimal beam waist thickness of the parabolic focus
425 widens near the edges of the confocal parameter with a factor $\sqrt{2}$. Consequently the light
426 plane has no constant thickness and thus no constant sectioning resolution. Furthermore, a
427 trade-off exists between the length of the confocal parameter and the thickness of the
428 plane. Large(r) macroscopic samples require a large confocal parameter and consequently a
429 thick sectioning plane and low sectioning resolution. Buytaert and Dirckx resolved this
430 problem in 2007 by line-scanning the sample across the minimal beam waist, and stitching
431 the section image columns together [7]. In this way, the confocal parameter is allowed to be
432 small, producing a thin sectioning plane and high sectioning resolution. Their
433 implementation was called High-Resolution OPFOS or HR-OPFOS. The newest version of HR-
434 OPFOS incorporates bi-directional sheet illumination as in Ultramicroscopy, cf. Figure 2 [4].
435

436 In 2008, three new LSFM versions were developed. Holekamp et al. fixed the light sheet
437 illumination unit to the observation objective [25]. This implementation was referred to as
438 Objective-Coupled Planar Illumination (OCPI) used for living brain imaging. Dunsby et al.
439 used a one high numeric aperture lens in his Oblique Plane Microscope (OPM) to both
440 illuminate the sample with an oblique light sheet and observe the fluorescence [26]. Finally,
441 Keller et al. introduced a new method to generate a light sheet. A tilting mirror rapidly scans
442 a micrometer thin *spherical* focus of laser light into a plane [27]. The method is called Digital
443 Scanned Laser Light Sheet Fluorescence Microscopy (DSLIM).
444

445 Thin-Sheet Laser Imaging Microscopy (TSLIM) by Santi et al. incorporates many improved
446 features of the previous devices [28], namely the bi-directional light-sheet illumination from
447 Ultramicroscopy; the image stitching idea from HR-OPFOS; and the combination of
448 cylindrical lenses with aberration corrected objectives from mSPIM.
449

450 Finally Mertz and Kim developed the HiLo LSFM system [29]. This DSLM-based device
451 counters sample-induced scattering and aberrations that broaden the thickness of the sheet
452 illumination. Through sequential uniform and structured sheet illumination, out-of-focus
453 background can be identified and rejected in post-processing, improving the image quality.
454

455 **Commercial devices**

456 The long lasting lack of a commercial LSFM device is responsible for the many different
457 implementations of the basic method, and for the unfamiliarity of researchers with the
458 technique in certain fields [11]. This is all about to change since now LSFM microscopes have
459 become commercially available.
460

461 *Carl Zeiss* showed a prototype of a commercial LSFM device, named SPIM, at the First LSFM
462 meeting in 2009 in Dresden (Germany). *Zeiss* is still preparing the launch of their system, but
463 *LaVision BioTec* already launched the Ultramicroscope (in collaboration with Dodt) near the
464 end of 2009 at Neuroscience in Chicago (US). The samples are limited to less than one cubic
465 centimeter and require clearing. The device is optimized to image juvenile mouse brains, and
466 complete mouse and fruit fly embryos. *LaVision* acknowledges the initial Ultramicroscopy
467 idea by Zsigmondy, and OPFOS by Voie as being the first tissue microscopy implementation.

468
469

470 **Conclusions**

471
472 We have shown with several applications that the OPFOS (and derived) methods, better
473 known as Light Sheet based Fluorescence Microscopy or LSFM, are a valuable addition for
474 sectional imaging and three-dimensional modeling of anatomic structures. LSFM has the
475 major advantage that the virtual slices are automatically and perfectly aligned, making it
476 easy to generate 3-D models from them. Microscopy techniques are either focusing on
477 flexibility, imaging depth, speed or resolution. LSFM has all these benefits according to
478 device manufacturers and the LSFM scientific community. Specimens containing both bone
479 and soft tissue and ranging from microscopic till small macroscopic in size, can be studied
480 with LSFM, with application in biomedical and life sciences. This microscopy method is
481 relatively new, conceptually simple but powerful. Researchers can easily build their own
482 setup, and even the first commercial devices are becoming available.

483
484

485 **Acknowledgments**

486
487 We thank A. Voie, P. Santi and U. Schröer for sharing information on OPFOS, the LSFM field
488 and the commercial Ultramicroscope device. We gratefully acknowledge the financial
489 support of
490 the Research Foundation – Flanders (FWO),
491 the Fondation belge de la Vocation,
492 the University of Antwerp,
493 and the GOA project (01G01908) of Ghent University.

494
495
496
497
498
499
500
501
502
503
504
505
506
507

508 **References**

- 509 [1] A.H. Voie, D.H. Burns, and F.A. Spelman, "Orthogonal-plane fluorescence optical
510 sectioning: three-dimensional imaging of macroscopic biological specimens.," *Journal*
511 *of microscopy*, vol. 170, 1993, pp. 229-236.
- 512 [2] W. Spalteholz, *Über das Durchsichtigmachen von menschlichen und tierischen*
513 *Präparaten*, Verlag Hirzel, 1911.
- 514 [3] H. Siedentopf and R.A. Zsigmondy, "Über Sichtbarmachung und Größenbestimmung
515 ultramikroskopischer Teilchen, mit besonderer Anwendung auf Goldrubingläser,"
516 *Annalen der Physik*, vol. 315, 1903, pp. 1-39.
- 517 [4] J.A.N. Buytaert and J.J.J. Dirckx, "Tomographic imaging of macroscopic biomedical
518 objects in high resolution and three dimensions using orthogonal-plane fluorescence
519 optical sectioning.," *Applied optics*, vol. 48, Feb. 2009, pp. 941-918.
- 520 [5] J. Huisken, J. Swoger, F.D. Bene, J. Wittbrodt, and E.H.K. Stelzer, "Live Embryos by
521 Selective Plane Illumination Microscopy," *Science*, vol. 305, 2004, pp. 1007-1009.
- 522 [6] J. Huisken and D.Y.R. Stainier, "Even fluorescence excitation by multidirectional
523 selective plane illumination microscopy (mSPIM).," *Optics letters*, vol. 32, Sep. 2007,
524 pp. 2608-2610.
- 525 [7] J.A.N. Buytaert and J.J.J. Dirckx, "Design and quantitative resolution measurements of
526 an optical virtual sectioning three-dimensional imaging technique for biomedical
527 specimens, featuring two-micrometer slicing resolution.," *Journal of biomedical*
528 *optics*, vol. 12, 2007, p. 014039.
- 529 [8] H.-U. Dodt, U. Leischner, A. Schierloh, N. Jahrling, C.P. Mauch, K. Deininger, J.M.
530 Deussing, M. Eder, W. Zieglgansberger, and K. Becker, "Ultramicroscopy: three-
531 dimensional visualization of neuronal networks in the whole mouse brain," *Nature*
532 *methods*, vol. 4, 2007, pp. 331-336.
- 533 [9] R. Hofman, J.M. Segenhout, J.A.N. Buytaert, J.J.J. Dirckx, and H.P. Wit, "Morphology
534 and function of Bast's valve: additional insight in its functioning using 3D-
535 reconstruction.," *European archives of oto-rhino-laryngology*, vol. 265, Feb. 2008, pp.
536 153-157.
- 537 [10] J. Buytaert, E. Descamps, D. Adriaens, and J. Dirckx, "Orthogonal-Plane Fluorescence
538 Optical Sectioning : a technique for 3-D imaging of biomedical specimens,"
539 *Microscopy: Science, Technology, Applications and Education*, A. Méndez-Vilas and J.
540 Díaz, eds., FORMATEX, 2010, pp. 1356-1365.
- 541 [11] P.A. Santi, "Light sheet fluorescence microscopy: a review," *The journal of*
542 *histochemistry and cytochemistry : official journal of the Histochemistry Society*, vol.
543 59, Feb. 2011, pp. 129-138.

- 544 [12] A.H. Voie, "Imaging the intact guinea pig tympanic bulla by orthogonal-plane
545 fluorescence optical sectioning microscopy.," *Hearing research*, vol. 171, Sep. 2002,
546 pp. 119-128.
- 547 [13] S.P. Tinling, R.T. Giberson, and R.S. Kullar, "Microwave exposure increases bone
548 demineralization rate independent of temperature.," *Journal of microscopy*, vol. 215,
549 Sep. 2004, pp. 230-235.
- 550 [14] C.F.A. Culling, "Spalteholz Technique," *Handbook of Histopathological and*
551 *Histochemical Techniques*, Butterworths, 1974, pp. 550-552.
- 552 [15] V. Ermolayev, M. Friedrich, R. Nozadze, T. Cathomen, M. a Klein, G.S. Harms, and E.
553 Flechsig, "Ultramicroscopy reveals axonal transport impairments in cortical motor
554 neurons at prion disease.," *Biophysical journal*, vol. 96, Apr. 2009, pp. 3390-8.
- 555 [16] J.A.N. Buytaert, W.H.M. Salih, M. Dierick, P. Jacobs, and J.J.J. Dirckx, "Realistic 3-D
556 computer model of the gerbil middle ear, featuring accurate morphology of bone and
557 soft tissue structures," *JARO-Journal of the Association for Research in*
558 *Otolaryngology*, vol. submitted, 2011.
- 559 [17] S. Van Wassenbergh, G. Roos, A. Genbrugge, H. Leysen, P. Aerts, D. Adriaens, and A.
560 Herrel, "Suction is kid' s play: extremely fast suction in newborn seahorses.," *Biology*
561 *letters*, vol. 5, Apr. 2009, pp. 200-203.
- 562 [18] R. Hofman, J.M. Segenhout, and H.P. Wit, "Three-dimensional reconstruction of the
563 guinea pig inner ear, comparison of OPFOS and light microscopy, applications of 3D
564 reconstruction," *Journal of microscopy*, vol. 233, Feb. 2009, pp. 251-257.
- 565 [19] J. Lane and Z. Ráliš, "Changes in dimensions of large cancellous bone specimens during
566 histological preparation as measured on slabs from human femoral heads," *Calcified*
567 *Tissue International*, vol. 35, 1983, p. 1-4.
- 568 [20] A.H. Voie and F.A. Spelman, "Three-dimensional reconstruction of the cochlea from
569 two-dimensional images of optical sections," *Computerized Medical Imaging and*
570 *Graphics*, vol. 19, 1995, p. 377-384.
- 571 [21] E. Fuchs, J. Jaffe, R. Long, and F. Azam, "Thin laser light sheet microscope for microbial
572 oceanography.," *Optics express*, vol. 10, Jan. 2002, pp. 145-54.
- 573 [22] R.A. Zsigmondy, "Properties of colloids," *Nobel lecture in chemistry*, 1926, pp. 1-13.
- 574 [23] E.H.K. Stelzer, S. Lindek, S. Albrecht, R. Pick, G. Ritter, N.J. Salmon, and R. Stricker, "A
575 new tool for the observation of embryos and other large specimens: confocal theta
576 fluorescence microscopy," *Journal of microscopy*, vol. 179, 1995, p. 1-10.
- 577 [24] S. Lindek and E.H.K. Stelzer, "Confocal theta microscopy and 4Pi-confocal theta
578 microscopy," *Proceedings of SPIE, Vol.2184: Three-Dimensional Microscopy*, SPIE
579 International Society for Optical Engineering, 1994, p. 188-188.

- 580 [25] T.F. Holekamp, D. Turaga, and T.E. Holy, "Fast three-dimensional fluorescence imaging
581 of activity in neural populations by objective-coupled planar illumination microscopy,"
582 *Neuron*, vol. 57, Mar. 2008, p. 661–672.
- 583 [26] C. Dunsby, "Optically sectioned imaging by oblique plane microscopy.," *Optics*
584 *express*, vol. 16, Dec. 2008, pp. 20306-16.
- 585 [27] P.J. Keller, A.D. Schmidt, J. Wittbrodt, and E.H.K. Stelzer, "Reconstruction of zebrafish
586 early embryonic development by scanned light sheet microscopy.," *Science (New York,*
587 *N.Y.)*, vol. 322, Nov. 2008, pp. 1065-9.
- 588 [28] P.A. Santi, S.B. Johnson, M. Hillenbrand, P.Z. GrandPre, T.J. Glass, and J.R. Leger,
589 "Thin-sheet laser imaging microscopy for optical sectioning of thick tissues,"
590 *BioTechniques*, vol. 46, Apr. 2009, pp. 287-94.
- 591 [29] J. Mertz and J. Kim, "Scanning light-sheet microscopy in the whole mouse brain with
592 HiLo background rejection," *Journal of biomedical optics*, vol. 15, 2011, p. 016027.
- 593